RSC Advances

PAPER

Cite this: *RSC Adv.*, 2016, **6**, 41861

Core–sheath structured electrospun nanofibrous membranes for oil–water separation†

Wenjing Ma,‡[a] Qilu Zhang,‡[b] Sangram Keshari Samal,‡[c] Fang Wang,[a] Buhong Gao,[d] Hui Pan,[a] Haijun Xu,[a] Jianfeng Yao,[a] Xianxu Zhan,[e] Stefaan C. De Smedt*[c] and Chaobo Huang*[af]

Received 9th March 2016
Accepted 17th April 2016

DOI: 10.1039/c6ra06224e

www.rsc.org/advances

In recent years, both the increasing frequency of oil spill accidents and the urgency to deal seriously with industrial oil-polluted water, encouraged material scientists to design highly efficient, cost effective oil–water separation technologies. We report on electrospun nanofibrous membranes which are composed of core–sheath structured cellulose-acetate (CA)–polyimide (PI) nanofibers. On the surface of the CA–PI fibers a fluorinated polybenzoxazine (F-PBZ) functional layer, in which silica nanoparticles (SNPs) were incorporated, has been applied. Compared with F-PBZ/SNP modified CA fibers reported before for the separation of oil from water, the PI-core of the core–shell F-PBZ/SNP/CA–PI fibers makes the membranes much stronger, being a significant asset in their use. Nanofibrous membranes with a tensile strength higher than 200 MPa, a high water contact angle of 160° and an extremely low oil contact angle of 0° were obtained. F-PBZ/SNP/CA–PI membranes seemed very suitable for gravity-driven oil–water separation as fast and efficient separation (>99%) of oil from water was achieved for various oil–water mixtures. The designed core–sheath structured electrospun nanofibrous membranes may become interesting materials for the treatment of industrial oil-polluted water.

1. Introduction

Oil spill accidents, which often occur upon exploitation, transportation, utilization and storage of oil,[1] do not only result in waste of resources but also seriously threaten the environment.[2–9] Besides oil spill accidents, oily wastewater, as produced by many industries,[10–16] has become one of the most common pollutants in the world, explaining why more and more material scientists focus on oil–water separation technologies. Some rather conventional techniques, such as adsorption,[17] gravity separation,[18] biological treatment,[19] sedimentation under centrifugal field[20] and electro-coagulation[21] are commonly used for oil–water separation. However, disadvantages such as low efficiency, high operation costs and generation of additional pollutants have greatly limited their wide applications. Membrane separation has been proved to be an effective technique to separate oil–water mixtures and has become widely adopted in food processing, pharmaceutical, desalination and fuel cell industries.[22–28]

Electrospinning is a versatile technique that allows creating nonwoven mats made of continuous fibers with diameters ranging from nanometers to a few micrometers.[29–31] Electrospun nanofibrous membranes show great potential in membrane filtration technology as they are mostly highly porous with an interconnected pore structure, which explains their large surface/volume ratio.[32–36] Electrospun nanofibrous membranes made from both polymers like polystyrene (PS),[37] polycaprolactone (PCL),[38] poly(methylmethacrylate),[39] polyurethane (PU)[40] and inorganic silica[41] have been designed for oil–water separation. Lin *et al.* developed PS–PU composite fibers with a high specific surface *via* co-axial electrospinning; such fibers showed oil sorption capacities of 64 and 48 g g^{-1} for motor oil and sunflower seed oil, respectively, being 2 to 3 times higher than the oil sorption capacity of conventional polypropylene (PP) fibers.[42] In another study by Shang *et al.* a superhydrophobic and super-oleophilic nanofibrous membrane was made from cellulose-acetate (CA) nanofibers modified with a fluorinated polybenzoxazine (F-PBZ) layer in which silica nanoparticles (SNPs) were incorporated; thus obtained nanofibrous membranes allowed fast and efficient separation of

[a]*College of Chemical Engineering, Nanjing Forestry University (NFU), Nanjing, 210037 P. R. China. E-mail: chaobo.huang@njfu.edu.cn*

[b]*Laboratory of Polymer Chemistry, Department of Chemistry, University of Helsinki, P.O. Box 55, 00014, Finland*

[c]*Lab General Biochemistry & Physical Pharmacy, Department of Pharmaceutics, Ghent University, Belgium*

[d]*Advanced Analysis & Testing Center, Nanjing Forestry University, Nanjing 210037, P. R. China*

[e]*Research Institute of Dehua TB New Decoration Material, Zhejiang Province, China*

[f]*Jiangsu Key Lab of Biomass-based Green Fuels and Chemicals, Nanjing, 210037 P. R. China*

† Electronic supplementary information (ESI) available: Detailed synthesis rute of BAF-tfa, FT-IR, ^{1}H NMR, ^{19}FNMR, set up for electrospinning CA–PI nanofiber membranes and orthogonal experiment scheme. See DOI: 10.1039/c6ra06224e

‡ These authors contributed equally to this work.

dichloromethane/water mixtures.[43] Che *et al.*[44] fabricated smart nanostructured electrospun poly(methylmethacrylate)-*co*-poly(*N*,*N*-dimethylaminoethyl methacrylate) membranes which can switch oil/water wettability by reacting with CO_2/N_2. In another study, polysulfone membranes containing silica nanoparticles were reported for oil–water separation;[45] the presence of the silica nanoparticles improved the flux through the membranes.

While most of the reported electrospun nanofibrous membranes show excellent oil–water separation properties, they often suffer from a poor mechanical stability which significantly hinders their potential in industrial applications. In this work we aimed to design sufficiently strong super-hydrophobic/super-oleophilic membranes based on high-strength core–sheath cellulose-acetate–polyamide (CA–PI) nanofibers modified with fluorinated poly-benzoxazine and silica nanoparticles (F-PBZ/SNP). As outlined in Scheme 1, co-axial electrospinning of CA with polyamide acid was performed to fabricate high strength core–sheath structured CA–PAA nanofibers which were subsequently imidizated resulting in CA–PI fibers, being CA fibers with a polyimide (PI) core. Fluorinated benzoxazine, namely 2,2-bis(3-*m*-trifluoromethylphenyl-*l*-3,4-dihydro-2*H*-1,3-benzoxazinyl) propane (BAF-tfa) was then *in situ* polymerized in the presence of silica nanoparticles forming a hydrophobic polymeric layer on the surface of the CA–PI fibers. The combination of the core–sheath structure of the fibers and the modification of their surface with F-PBZ/SNP resulted in strong nanofibrous membranes with an excellent super-hydrophobic/super-oleophilic surface showing promising features for gravity driven oil–water separation.

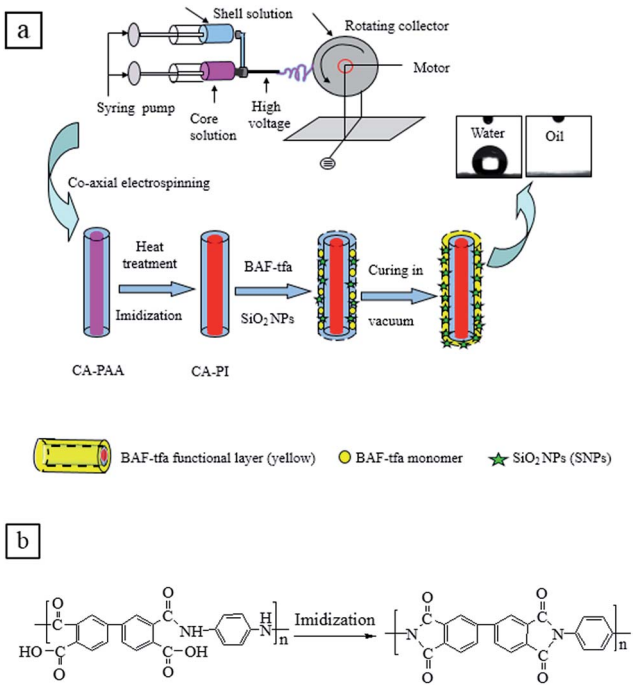

Scheme 1 (a) F-PBZ/SNP modified CA–PI nanofibrous membranes prepared through co-axial electrospinning: cellulose-acetate (CA), polyamide acid (PAA), polyimide (PI); (b) shows the imidization of PAA.

2. Experimental

2.1. Materials

Bisphenol AF, paraformaldehyde (POM), 3-(trifluoromethyl) aniline, hydrophobic silica (SiO_2) nanoparticles (7–40 nm) and hexadecyl trimethyl ammonium bromide were provided by Shanghai Aladdin Industrial Corporation. *N*,*N*-Dimethylacetamide (DMAc), dichloromethane (DCM), acetone, trichloromethane, anhydrous calcium chloride, *n*-butyl acetate and sodium hydroxide were purchased from Nanjing Chemical Reagents. Cellulose-acetate (M_w = 40 000) was purchased from Sinopharm Chemical Reagent. 3,3′,4,4′-Biphenyl tetracarboxylic dianhydride (BPDA, from Changzhou Sunlight Pharmaceutical) and *p*-phenylenediamine (PDA, from Shanghai Aladdin Industrial Corporation) were sublimated under vacuum before use. All chemicals and solvents were used as received, unless otherwise stated.

2.2. Synthesis of 2,2-bis(3-*m*-trifluoromethylphenyl-*l*-3,4-dihydro-2*H*-1,3-benzoxazinyl)propane (BAF-tfa)

BAF-tfa was synthesized using *p*-phenylenediamine, paraformaldehyde (POM) and 3-(trifluoromethyl) aniline through Mannich reaction, as shown in Fig. S1.† 14.7 g bisphenol AF (BAF), 5.3 g paraformaldehyde and 14.1 g 3-(trifluoromethyl) aniline were stirred in a four necked round bottom flask equipped with a condenser with electric mixer under N_2 environment for 30 min. The reaction temperature was gradually increased to 105 °C. After 2 h of reaction the viscosity of the mixture began to increase. The reaction mixtures were dissolved in 200 mL trichloromethane after cooling down to room temperature. The resulting solution was washed successively using 2.0% aqueous sodium hydroxide and deionized water followed by drying with anhydrous calcium chloride and filtration. Subsequently the solvent was evaporated under vacuum and the product was dried at 50 °C for 24 h to obtain BAF-tfa powder. ^{1}HNMR spectrum (500 MHz) in $CDCl_3$ and DMSO-d6 and ^{19}FNMR spectrum (500 MHz) in $CDCl_3$ were collected and shown in Fig. S2.† Fig. S3† shows the FT-IR spectrum of the thus obtained BAF-tfa.

2.3. Synthesis of polyamide acid (PAA)

Polyamide acid (PAA) was synthesized from BPDA and PDA through low temperature polycondensation, as shown in Fig. S4.† BPDA (2.9421 g) and 1.0814 g (PDA) were dissolved in 40 mL DMAc in a four-necked round bottom flask equipped with a mechanical stirrer under nitrogen environment at −5 °C. The reaction was stopped after 4 hours and the molecular weight was measured by GPC.

2.4. Electrospun polyimide (PI) nanofibrous membranes

PAA nanofibrous membranes were prepared using 3 wt% PAA solutions in DMAc containing 1 wt% hexadecyl trimethyl ammonium bromide to enhance the conductivity. Fig. S5† shows the electrospinning setup: electrospinning occurred at a voltage of 25 kV (+15, −10 kV), the PAA solution was fed from a syringe into a needle at a flow rate of 1 mL h^{-1}. PAA nanofibrous membranes were collected on an earthed rotating flywheel (fiber

collector), 30 cm in diameter. The flywheel rotated at 1500 rpm which allowed to generate membranes with aligned fibers. The FT-IR spectrum of the resulting PAA membrane is shown in Fig. S6, ESI.† PI nanofibrous membranes were obtained by imidization of the PAA membranes through heat treatment[46] (150 °C/1 h, 200 °C/1 h, 250 °C/1 h, 300 °C/1 h, 350 °C/30 min).

2.5. Preparation of cellulose-acetate (CA) nanofibrous membranes

CA nanofibrous membranes were prepared using a 7.5% (w/v) CA solution (in DCM/acetone (2 : 1, v/v)) which was loaded in the syringe and injected through the metal needle (1 mL h^{-1}). Electrospinning occurred using the setup described in Section 2.4.

2.6. Co-axial electrospinning of CA–PI nanofibrous membranes

The co-axial electrospinning process was performed using a 3 wt% PAA solution (in DMAc) to make the core and a 7.5% (w/v) CA solution (in DCM/acetone; (2 : 1, v/v)) to form the sheath. An electrospinning setup similar as described above for CA and PI spinning was used, except the use of two syringe pumps and a spinneret consisting of two chambers. The nozzle included two circular channels, the configuration is shown in Fig. S7.† The applied voltage equalled 25 kV (+15, −10 kV), while the distance between the spinneret and the collector was 13 cm. The needle of the co-axial electrospinning with an inner diameter of 0.51 mm and an outer diameter of 1.25 mm was used. The flow rate of both the core and sheath solution was 1 mL h^{-1}. The electrospun CA–PAA nanofibers were collected as nonwoven sheets on the rotating roller (1500 rpm). The obtained CA–PAA nanofibers were subsequently imidizated through heat treatment (150 °C/2 h, 200 °C/3 h, 250 °C/1 h and 260 °C/1 h).

2.7. Fabrication of F-PBZ/SNP modified CA, PI and CA–PI nanofibrous membranes

The F-PBZ/SNP modified CA, PI, and CA–PI nanofibrous membranes were fabricated by first dipping the electrospun CA, PI or CA–PI membranes in *n*-butyl acetate solutions with various concentrations of BAF-tfa and SNPs. The membranes were oven dried for 2 h at 60 °C, followed by *in situ* polymerization of the BAF-tfa monomers at 190 °C in vacuum for 3 h. The thus obtained membranes modified using *x* wt% BAF-tfa/butyl acetate solutions were denoted as F-PBZ-*x*. Similarly, the F-PBZ/SNP modified CA, PI and CA–PI samples were denoted as F-PBZ-*x*/SNP-*y*/CA, F-PBZ-*x*/SNP-*y*/PI and F-PBZ-*x*/SNP-*y*/CA–PI, respectively, where *x* and *y* indicate the used concentrations of BAF-tfa (*x* wt%) and SNPs (*y* wt%), respectively.

2.8. Instrumentation

The nanofibrous membranes were fabricated using commercially available electrospinning equipment (FM1206, Beijing Future Material Sci-tech, China). ^{1}H NMR spectra were recorded by a Bruker Avance 400. Fourier transform infrared (FT-IR) spectra were recorded with a Nicolet 8700 FT-IR spectrometer. The morphology of the fiber composites was characterized using a JEM-2010 transmission electron microscope with accelerating voltage of 120 kV. Samples were stained with 0.2% phosphotungstic acid. The morphology of the membranes was further examined using field emission scanning electron microscopy (FE-SEM, S-4800, Hitachi Ltd., Japan). Water contact angle (WCA) and oil contact angle (OCA) measurements were performed using a contact angle instrument (JC2000D1, Shanghai Zhong Chen digital technic apparatus). The mechanical properties of the membranes were evaluated on an electronic universal testing machine (UTM6502, Shenzhen Sans Technology Stock, China). Thermogravimetric analysis was performed using Thermal Gravimetric Analyzer (TGA Q5000-IR, TA Instruments). Gel Permeation Chromatography (GPC) (Agilent Technologies, Germany) was conducted to investigate the molecular weight of PAA. The roughness parameters (R_a) of the membranes were measured using white light interferometer (ContourGT-K, Bruker, USA). N_2 adsorption–desorption isotherms, pore size distributions (PSD) and pore volume were investigated using an Autosorb-iQ2 physisorption analyzer (Quantachrome, USA).

2.9. Oil–water separation performance of the membranes

To assess the oil–water separation performance of the membranes, 20 mL of an oil/water mixture (1/1; v/v) was poured into a commercially available separation device (mobile phase filter, Synthware, China; see Fig. 8a). The oil–water mixtures were obtained by mixing 10 mL oil and 10 mL water in a beaker and simply shaking by ultrasound. The flux (F) of the oil through the membrane was calculated as follows:

$$F = \frac{\nu}{A\Delta t} \tag{1}$$

V (L) being the volume of oil which passes through the membrane, A (m^2) the (surface) area of the membrane (*i.e.* 56.25 $\times$ 10^{-6} m^2) and Δt (h) the filtration time. The 'separation efficiency' was calculated from:

$$\eta = \frac{V_1}{V_0} \times 100 \tag{2}$$

V_0 being the volume of water used to prepare the oil/water mixture, V_1 being the volume of water recovered after the separation process.

2.10. Porosity of the membranes

The porosity (P) of the electrospun nanofibrous membranes was calculated following the work of Liu *et al.*:[47]

$$\rho_{\text{membrane}} = \frac{\text{mass}_{\text{membrane}}}{\text{area}_{\text{membrane}} \times \text{thickness}_{\text{membrane}}} \tag{3}$$

$$\rho_{\text{film}} = \frac{\text{mass}_{\text{film}}}{\text{area}_{\text{film}} \times \text{thickness}_{\text{film}}} \tag{4}$$

$$p = \left(1 - \frac{\rho_{\text{membrane}}}{\rho_{\text{film}}}\right) \times 100\% \tag{5}$$

where ρ_{membrane} and ρ_{film} are the density of respectively the electrospun nanofibrous membrane and the corresponding 'polymer

film' obtained upon evaporating the solvent of a 1.5 mL polymer solution spread on a microscopy glass. Note that the thickness of the nanofibrous membranes and the polymer films were measured using digital micrometre (Master proof, Germany).

3. Results and discussions

3.1. Electrospinning and characterization of core–sheath structured CA–PI nanofibers

Fig. 1 shows the stress–strain curves of CA, PI and CA–PI nanofibrous membranes stretched in the oriented direction (0.5 × 4 cm and thickness of 40 μm). A typical linear stress–strain behavior appeared before the breaking of the membranes. This deformation behavior could be explained as follows. Under the action of an external load, the non-aligned nanofibers in the membranes were first compelled to be aligned along the stress direction, which explains the initial non-linear behavior. The linear stress–strain behavior upon further increasing the tensile stress is due to the intrinsic (elastic) properties of the nanofibers.

Breaking of the aligned CA-nanofibers/CA-membranes seemed to occur already at 10 MPa membranes occurred at a much higher tensile stress (400 MPa); the high mechanical properties of the PI-membranes can be ascribed to (insert) which may be partially explained by the low molecular weight of CA ($M_w = 40,000$). In clear contrast, breaking of PI-the aromatic structure of polyimide and the high molecular weight ($M_w = 1.0 \times 10^8$) resulting from the low-temperature polymerization process.[48,49] In addition, polymer chain orientation and/or crystallization may happen during the high temperature imidization process, which may also contribute to the high strength of the membranes. Fig. 1 shows that CA–PI membranes have a tensile strength of 230 MPa, which is about 20 times higher than the tensile strength of the CA-membranes. The tensile strength was smaller when the membrane stretched in the vertical direction (Fig. S8†).

Transmission electron microscope (TEM) was applied to characterize the structure and morphology of the electrospun

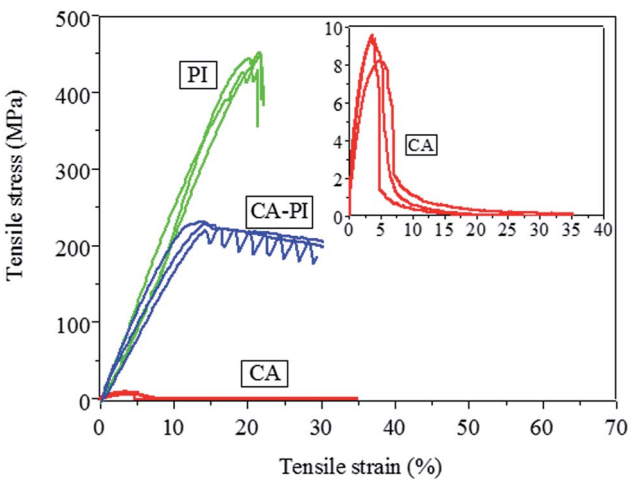

Fig. 1 Stress–strain behavior of CA, PI, CA–PI membranes. The insert shows the stress–strain behavior of CA.

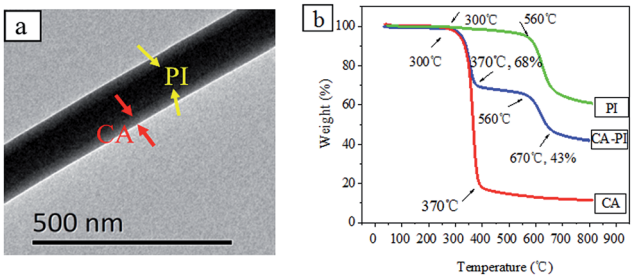

Fig. 2 (a) TEM image of a CA–PI nanofiber; (b) TGA on CA, PI, and CA–PI membranes.

nanofibers (Fig. 2a). The fibers obtained by co-axial electrospinning and subsequent imidization of PAA were very thin and showed a clear core–sheath structure; it looks like a PI wire (core) is present in a CA fiber (sheath). It is this core–sheath structure of the nanofibers which explains why CA–PI nanofibers perform mechanically so much better than CA-fibers.[50,51]

Subsequently, the thermal stability of the CA, PI and CA–PI nanofibrous membranes was studied by thermogravimetric analysis (TGA). As shown in Fig. 2b, PI-membranes were very stable upon heating and no decomposition took place until 560 °C (under nitrogen atmosphere). In contrast, CA-membranes started to decompose at about 300 °C and lost about 85% of their mass at 350 °C. Unlike CA- and PI-membranes, the degradation of CA–PI nanofibrous membranes was found to display a two-stage decomposition with a 37% mass loss between 300 and 370 °C followed by another 20% mass loss between 560 and 670 °C. The two steps in loosing mass could be ascribed to the decomposition of CA and PI fibers, respectively, which supports the above proposed core–sheath structure of the CA–PI nanofibers. Moreover, the stability of CA and CA–PI nanofibrous membranes at temperatures lower than 300 °C also confirms that the imidization step (Scheme 1) which occurred at 260 °C (during 30 min) did not damage the fibers.

3.2. *In situ* polymerization modification of electrospun nanofibrous membranes

To achieve electrospun nanofibrous membranes with a superhydrophobic/super-oleophilic surface suitable for oil–water separation, the fibers were coated with fluorinated polybenzoxazine (F-PBZ) *via in situ* polymerization. The resulting F-PBZ modified electrospun nanofibrous membranes were characterized by FE-SEM, as shown in Fig. 3d–f; images for pristine CA, PI, and CA–PI nanofibers were also shown for comparison (Fig. 3a–c). The figures show that the surface of uncovered CA nanofibrous membranes (Fig. 3a) is relatively rough, while PI and CA–PI nanofibers exhibit a relatively smooth surface, especially in case of PI. Comparing with Fig. 3a–c, the morphology of the nanofiber's surface did not change significantly upon F-PBZ modification. However, cross-linked polymer thin layer was evidenced after BAF-tfa modification confirming the successful *in situ* polymerization of BAF-tfa on the surface of CA, PI, and CA–PI nanofibers.

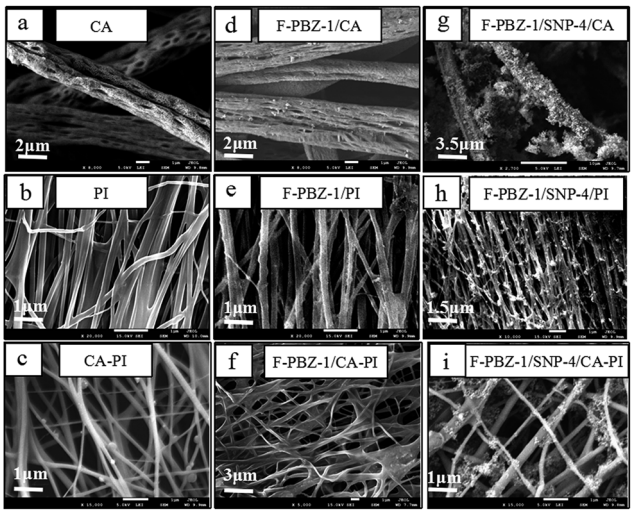

Fig. 3 FE-SEM images of electrospun fibrous mats.

The presence of an F-PBZ modified surface of CA, PI and CA–PI nanofibers could be confirmed by FT-IR spectroscopy (Fig. 4). As shown in Fig. 4a, the absorption peaks of CA around 1750, 1640 and 1050 cm^{-1} could be assigned to C=O, the stretching vibration of C–O–C and the wagging of C–O, respectively. In comparison with Fig. 4a(I), the spectrum of modified CA shown in Fig. 4a(II) displays peaks at 874, 945 and 1380 cm^{-1}, which correspond to the absorption of the oxazine ring, C–O–C and the triple substituted phenyl ring, indicating the presence of benzoxazine on the surface of CA. In Fig. 4b(I), the absorption peaks at 1716, 1771 and 1356 cm^{-1} were assigned to the stretching vibration of –COOH, –CONH and C–N, respectively, indicating successful electrospinning of PI. The absorption peaks of the oxazine ring, C–O–C and the triple substituted phenyl ring at 830, 945 and 1380 cm^{-1} in Fig. 4b(II) confirmed the modification of benzoxazine on the surface of PI. Similarly, the F-PBZ modification of CA–PI fibers could also be confirmed by the FT-IR spectra shown in Fig. 4c.[52]

After the surface modification of CA, PI and CA–PI electrospun nanofibrous membranes, the hydrophobicity and oleophilicity of the surface of the thus obtained membranes were characterized by contact angle measurements. As shown in Fig. 5a for modified CA fibers, the water contact angles (WCAs) increased upon increasing the BAF-tfa concentration. Adding 0.01 wt% of BAF-tfa monomer seemed already sufficient to increase the WCA from 0° to 128°. Such significant increase in hydrophobicity can be ascribed to the filling of BAF-tfa monomer between the CA nanofibers during mechanical stirring due to a typical polydisperse porous structure and a primary PSD in the range of 30–150 nm (Fig. S9†). Subsequent *in situ* polymerization of the monomers at 190 °C resulted in the formation of F-PBZ on the surface of the CA fibers, which provided the composite with a high hydrophobic surface due to the lower surface energy of $-CF_3$ on the polymer side chains.[53] Increasing the BAF-tfa (monomer) concentration resulted in a higher deposition of F-PBZ leading to a slight increase of the WCAs. However, at BAF-tfa concentrations higher than 1 wt%, the

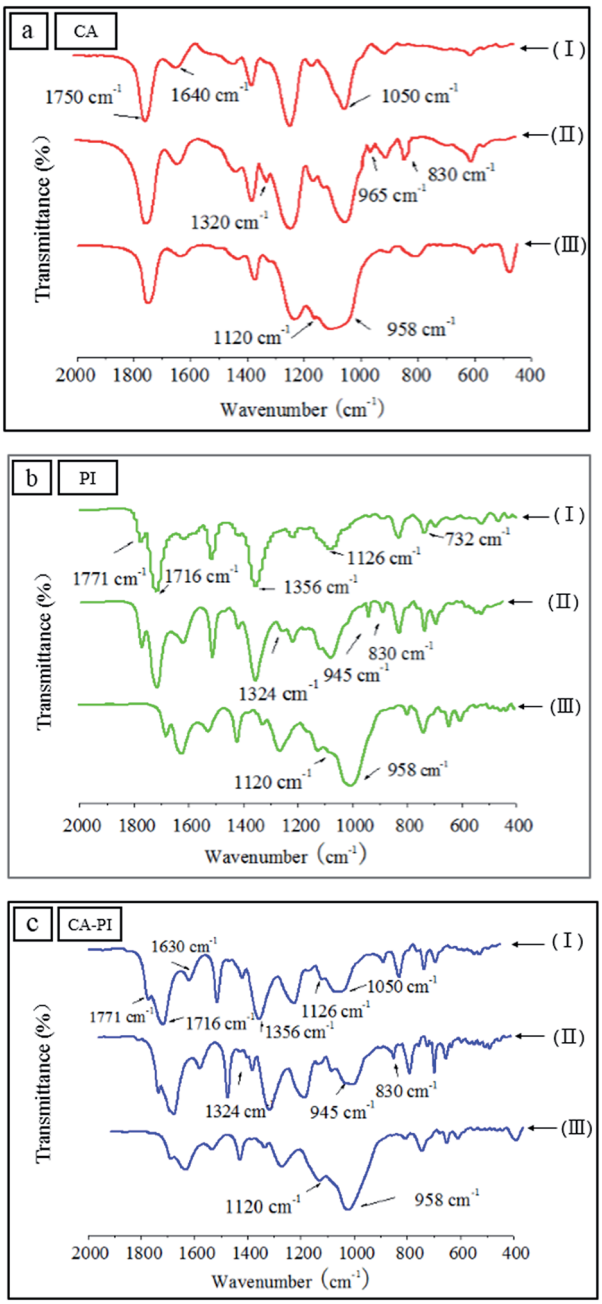

Fig. 4 FT-IR spectrograph of (a) CA, (b) PI and (c) CA–PI membranes. (I), (II) and (III) correspond to respectively pristine fibrous membranes, membranes modified with 1 wt% BAF-tfa and membranes modified with 1 wt% BAF-tfa and 4 wt% SNPs.

WCAs seemed to be lower. This may be explained by the fact that the surface wettability of nanofibrous membranes is influenced by both the surface free energy and the surface roughness. A (very) high amount of BAF-tfa may cause the filling of space among the nanofibers, thereby reducing the roughness of the membranes, with the increasing of the concentration of BAF-tfa, an decrease of R_a values of 1.689, 1.644, 1.625, 1.604, 1.447, 1.275 and 1.176 μm for the F-PBZ-0.01/CA–PI, F-PBZ-0.02/CA–PI, F-PBZ-0.05/CA–PI, F-PBZ-0.1/CA–PI, F-PBZ-0.5/CA–PI, F-PBZ-1/CA–PI and F-PBZ-4/CA–PI, respectively (Fig. S10†). The

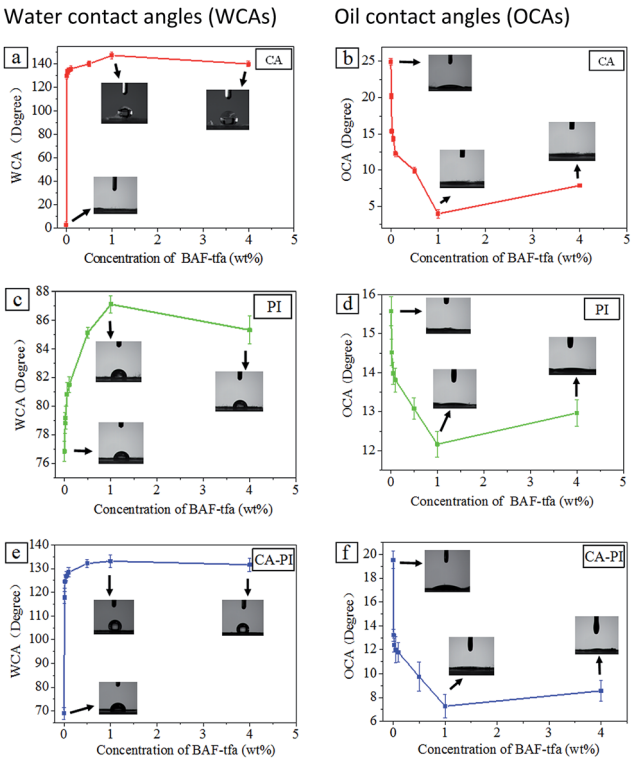

Fig. 5 WCAs (a, c, e) and OCAs (b, d, f) of CA (a and b), PI (c and d) and CA–PI (e and f) modified with different concentrations of BAF-tfa.

surface of modified PI nanofibrous membranes (Fig. 5c) was found to be much less hydrophobic than that of modified CA-membranes (Fig. 5a), which can be ascribed to the smooth surface of the PI fibers. The WCAs of modified core–sheath structured CA–PI nanofibrous membranes (Fig. 5e) seemed similar to the WCAs of modified CA-membranes; they seemed to be slightly less hydrophobic may be ascribed to the fact that the surface of CA–PI fibers seems less rough (compared to the surface of CA fibers; see Fig. 3i *versus* Fig. 3g).

Subsequently the oleophilicity of CA, PI and CA–PI nanofibrous membranes was characterized by OCA. As shown in Fig. 5b–f, CA, PI and CA–PI nanofibrous membranes were already oleophilic before BAF-tfa modification. Upon modification, the OCAs of the nanofibrous membranes gradually decreased. The lowest OCA values for CA, PI and CA–PI nanofibrous membranes, found at 1 wt% of BAF-tfa, were 2°, 12° and 5°, respectively, indicating that the membranes are superoleophilic; this is clearly attributed to the lipophilic benzene containing BAF-tfa that improves the wettability of the membranes by oil. Increasing BAF-tfa concentrations higher than 1 wt% reduced the surface roughness of the fibrous membranes, explaining the lowered oleophilicity.

Next, the stability and persistence of the surface modified PI and CA–PI nanofibrous membranes were evaluated. As shown in Fig. 6, the change in WCA of PI and CA–PI nanofibrous membranes turned out to be less than 4% in 300 days (stored in box at room temperature). The results indicate that the modified nanofibrous membrane composites seem stable, which is promising for the practical application of such membranes.

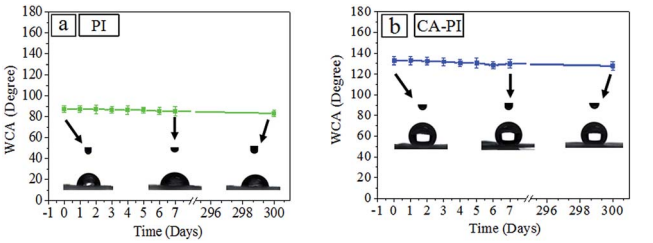

Fig. 6 WCAs of (a) PI and (b) CA–PI membranes (modified with 1 wt% BAF-tfa) stored for about one year (at room temperature).

3.3. *In situ* polymerization modification of electrospun nanofibrous membranes in the presence of silica nanoparticles

Nanoparticles have been widely used to fabricate fibers with 'functional' surfaces or to change the wettability of the fibers.[54–57] It has been reported as well that modification of the surface of the fibers with nanoparticles (*e.g.* SiO_2) can significantly improve the hydrophobicity of the surface.[58,59] To further optimize the properties of the BAF-tfa modified surfaces of the fibers for oil–water separation, silica nanoparticles were dispersed in the BAF-tfa/*n*-butyl acetate solution used to modify the CA, PI and CA–PI nanofibrous membrane surfaces. As shown in Fig. 3g–i, with SNPs in the F-PBZ layer, the morphology of the membranes remarkably changed, *i.e.* nanoscaled rough hierarchical 3D structures were clearly visible on the surface of the nanofibers. The SNPs were well-positioned on the surface of the nanofibers with negligible amount of SNPs present between the nanofibers. The successful incorporation of SNPs was confirmed by FT-IR spectroscopy. As shown in Fig. 4a(III)–c(III), the appearance of the characteristic vibration of Si–OH at 958 cm^{-1} and of Si–O–Si at 1120 cm^{-1} indicated the incorporation of SNPs in the nanofibrous membranes.

To find BAF-tfa and SNPs modified nanoporous membranes with optimal surface properties for oil–water separation, orthogonal experiments were performed with different concentrations of BAF-tfa monomer and SNPs (Fig. 7 and Table S1, ESI†). The results revealed that, at a given content of SNPs, the surface hydrophobicity of the modified membranes exhibit the same trend as seen for nanoparticle-free membranes, *i.e.* the surfaces became more hydrophobic at higher BAF-tfa loading (till a BAF-tfa concentration of 1 wt%; Fig. 7a–e). At a defined concentration of BAF-tfa, both the hydrophobicity (WCAs, Fig. 7a–e) and oleophilicity (OCAs, Fig. 7b–f) of the membranes could be improved by SNPs, as their surface became rougher. For CA membranes the highest WCA (166°) could be obtained by F-PBZ-1/SNP-4 modification. The core–sheath structured CA–PI nanofibrous membranes could be made super-hydrophobic (WCA of 160° and extremely low OCA) by the use of SNPs.

3.4. Gravity driven oil–water separation

To test the oil–water separation potential of F-PBZ-1/SNP-4/CA–PI membranes, a gravity driven oil–water separation experiment was performed, as schemed in Fig. 8. The separation device consisted of a F-PBZ-1/SNP-4/CA–PI membrane between two

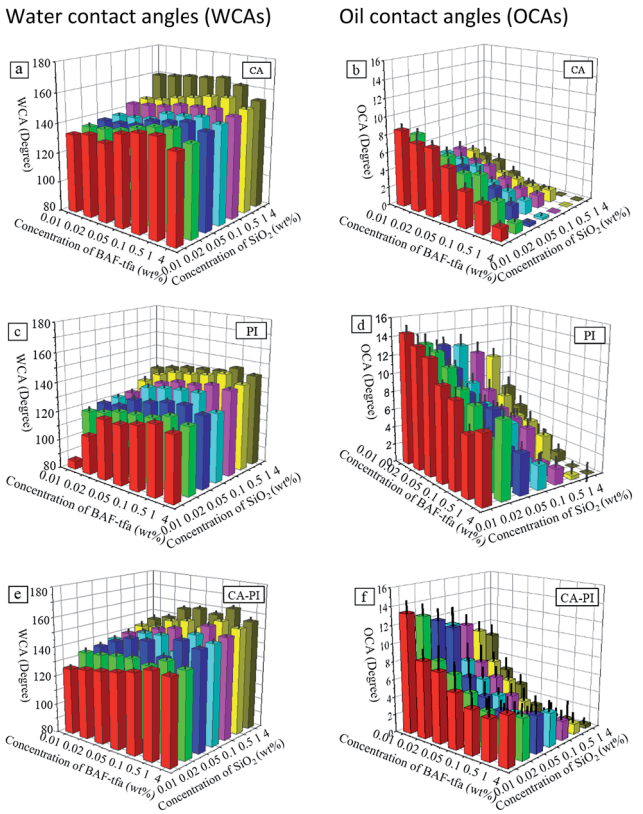

Fig. 7 WCAs (left) and OCAs (right) of CA (a and b), PI (c and d) and CA–PI (e and f) membranes modified with different concentrations of BAF-tfa monomer and SNPs.

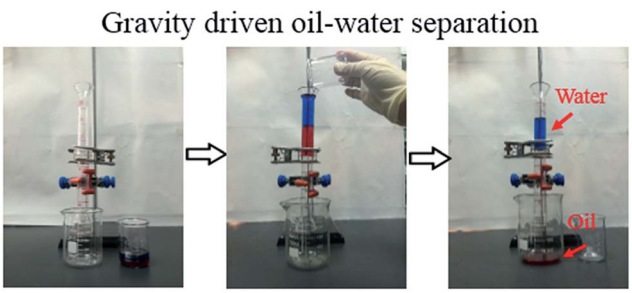

Fig. 8 Oil–water separation using F-PBZ-1/SNP-4/CA–PI nanofibrous membranes, the water and oil were dyed with respectively methylene blue and oil red.

glass tubes. Upon pouring a 20 mL mixture of oil dichloromethane (DCM) and water (50% v/v) the oil quickly passed through the membrane and reached the beaker, while all the water was retained by the membrane. It is worth noting that such a fast separation process (within 5 min) was only driven by the weight of the oil, thus without the use of extra energy that the oil phase need to be heavier (higher density) than water, then the oil can be well contacted with the membranes. Subsequently, optical microscopic images of the original oil–water mixture and the corresponding filtrate (Fig. S12†) as well as photograph of oil and water phase after separation centrifuge with 4000 rpm were collected (Fig. S13†). A very clear filtrate was

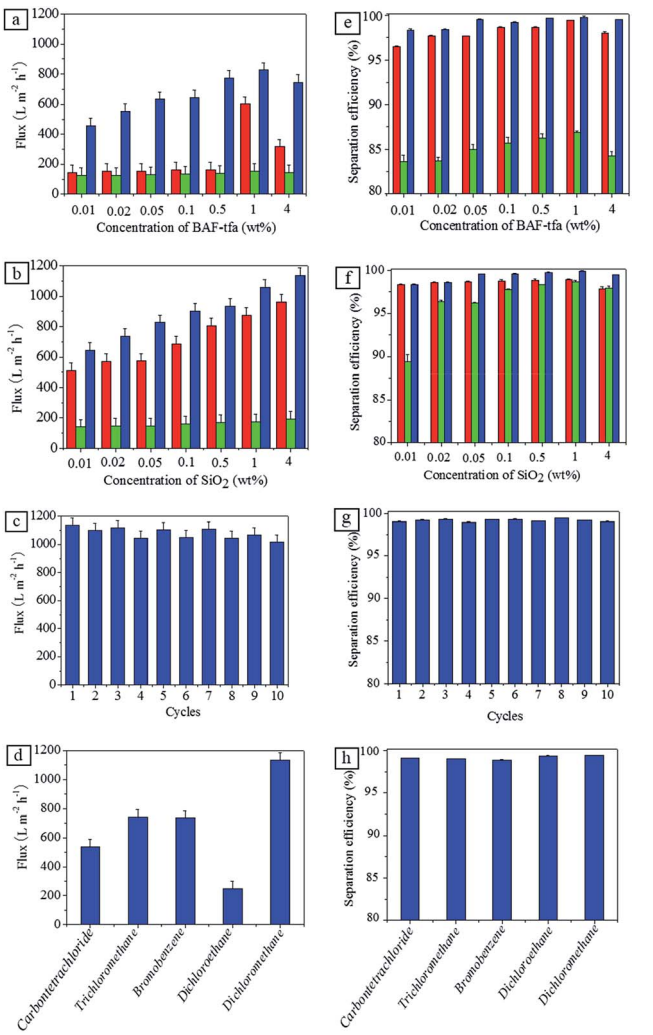

Fig. 9 (a–c) Flux of dichloromethane (DCM) through electrospun CA- (□), PI- (□) and core–sheath structured CA–PI (□) nanofibrous membranes. (d) Flux of various oil–water mixtures through F-PBZ-1/SNP-4/CA–PI membranes. (e–g) Separation efficiency of the membranes for dichloromethane–water mixtures. (h) Separation efficiency of F-PBZ-1/SNP-4/CA–PI membranes for various oil–water mixtures.

observed indicating that the F-PBZ-1/SNP-4/CA–PI membranes were highly efficient in separating oil from water for its type IV N_2 adsorption–desorption isotherms. In addition, typical mesopores were found in the membranes with a pore size of about 5–60 nm with a central size of ~36 nm. Significantly, the F-PBZ-1/SNP-4/CA–PI membranes possessed the pore volume of 0.2091 $cm^3\ g^{-1}$ (Fig. S14†), which provided a large number of porous channels that could enhance the liquid transport under the action of the capillary force that was conducive to improve the oil–water separation performance.

Subsequently we evaluated the flux of oil through the electrospun nanofibrous membranes in more detail. As shown in Fig. 9a and b, the flux of dichloromethane through CA–PI membranes is significantly higher than the one through (corresponding) CA- and PI-membranes, revealing attractive properties of the core–sheath structured CA–PI nanofibrous membranes.

Note that increasing the BAF-tfa and SNPs content clearly improved the flux through the CA–PI nanofibrous membranes, which could be (highly likely) ascribed to higher WCAs and lower OCAs, as also proposed by others.[60] For F-PBZ-1/SNP-4/CA–PI membranes the (dichloromethane) water flux even equalled 1136 $\pm$ 50 L m^{-2} h^{-1} which is significantly higher than the (typical) flux through commercial filtration membranes (20–200 L m^{-2} h^{-1} (ref. 61)) and the oil permeability through the membrane was 87.5% calculated according to comparing the volume of oil before and after separation. Note that upon repetitive use of the CA–PI membranes the flux of dichloromethane nearly changed (Fig. 9c), which indicates and excellent re-usability of the nanofibrous membranes we designed. Also, besides for DCM–water mixtures, as Fig. 9d shows, a high flux through CA–PI nanofibrous membranes was easily achieved as well for trichloromethane–water, carbontetrachloride–water and bromobenzene–water mixtures, indicating the versatility of the designed nanofibrous membranes. Significantly, different oil–water mixture compositions were carried out the oil–water separation (Fig. S15†), revealing all of these samples were well separated regardless of the different compositions of oil–water and the mixture with more water led to a higher separation speed (flux) due to the higher hydraulic pressure.

Fig. 9e and f shows the separation efficiency of the membranes (as defined by eqn (2) in Section 2.9) for dichloromethane-water mixtures. Clearly, the separation efficiency of the core–sheath structured CA–PI nanofibrous membranes is nearly 100%, independent on the concentration of SNPs and BAF-tfa, and outperforms the separation efficiency of (corresponding) PI-membranes.

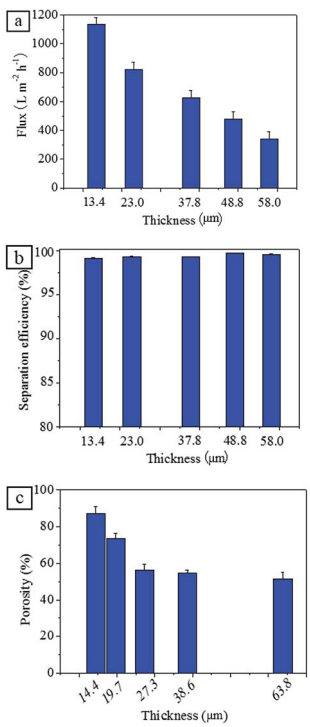

Fig. 10 (a) Flux of DCM through F-PBZ-1/SNP-4/CA–PI nanofibrous membranes with different thickness. (b) Separation efficiency of these membranes for dichloromethane–water mixtures and their porosity (c).

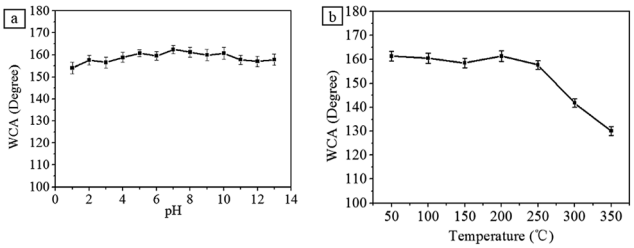

Fig. 11 WCAs of F-PBZ-1/SNP-4/CA–PI membranes. (a) In function of the pH of the water in the oil–water mixtures and (b) after calcination at different temperatures in air (for 10 min).

Fig. 9g indicates that, even after ten separation cycles, the separation efficiency of the CA–PI nanofibrous membranes remains over 98%; also, the CA–PI nanofibrous membranes show an excellent separation efficiency for the various oil–water mixtures (Fig. 9h).

For F-PBZ-1/SNP-4/CA–PI membranes we also tested the DCM–flux and separation efficiency of as a function of the membrane thickness (Fig. 10a and b). Thinner membranes were found to have a higher porosity (Fig. 10c) which may explain the higher flux through thin membranes (Fig. 10a). Note that the efficiency separation efficiency was not significantly affected by the membrane thickness (Fig. 10b).

To evaluate the potential of F-PBZ-1/SNP-4/CA–PI membranes for oil–water separation, WCAs were measured as a function of the pH of water (pH ranging from 1 to 13). Fig. 11a shows that, independent of the pH, the WCAs remain high (about 160°) indicating that the membranes are stable both under acid and alkali conditions. As Fig. 11b shows, the WCAs did not change after annealing the membranes at 250 °C for 10 min, suggesting that even under harsh conditions such membranes will remain functional. As Fig. 11b indicates, increasing the annealing temperature to 300 °C lowers the WCA to 142°, which may be due to the decomposition of nanofibers.

4. Conclusions

In summary, we have designed high strength super-hydrophobic and super-oleophilic nanofibrous membranes which seem very suitable for gravity driven oil–water separation. The membranes consist of electrospun core–sheath structured CA–PI nanofibers, having a F-PBZ functional layer incorporating SNPs at their surface. The core–sheath structured CA–PI nanofibers combine high mechanical properties from the PI fiber core and a rough surface from the CA sheath. Further modification of the surface of the CA–PI membranes by F-PBZ/SNP made the pristine CA–PI membranes super-hydrophobic and super-oleophilic. The optimized F-PBZ-1/SNP-4/CA–PI membranes show a fine hierarchical roughness, have a tensile strength of higher than 200 MPa, a high WCA of 160° and an extremely low OCA. Importantly, the nanofibrous membrane seemed very stable under various harsh conditions, like low and high pH, and high temperature. Finally, F-PBZ-1/SNP-4/CA–PI membranes seemed very suitable for gravity-driven oil–water separation as a fast (*i.e.* fluxes up to 1136 $\pm$ 50 L m^{-2} h^{-1}) and efficient separation (*i.e.* >99%) of water from

oil was achieved for certain oil–water mixtures, even after re-use of the membranes. The newly designed core–sheath structured electrospun nanofibrous membranes may become interesting materials for the treatment of oil–polluted water and oil spill clean-up processes.

Acknowledgements

Financial supports from the Jiangsu specially-appointed professorship program (Sujiaoshi [2012]34), the National Natural Science Foundation of China (No. 21301092, 31200451), Priority Academic Program Development of Jiangsu Higher Education Institutions (PAPD), Scientific Research Staring Foundation for the Returned Overseas Chinese Scholars and Ministry of Education of China, Jiangsu key lab of biomass-based green fuels and chemicals (JSBGFC14001) and the Fok Ying Tung Education Foundation (grant No. 141030) are acknowledged with gratitude. We also thank Advanced Analysis & Testing Center, Nanjing Forestry University for SEM characterization.

Notes and references

1 J. Albaiges, *Int. J. Environ. Anal. Chem.*, 2014, **94**, 1–3.
2 E. B. Kujawinski, M. C. Kido Soule, D. L. Valentine, A. K. Boysen, K. Longnecker and M. C. Redmond, *Environ. Sci. Technol.*, 2011, **45**, 1298–1306.
3 C. M. Reddy, J. S. Arey, J. S. Seewald, S. P. Sylva, K. L. Lemkau, R. K. Nelson, C. A. Carmichael, C. P. McIntyre, J. Fenwick and G. T. Ventura, *Proc. Natl. Acad. Sci. U. S. A.*, 2012, **109**, 20229–20234.
4 J. E. Kostka, O. Prakash, W. A. Overholt, S. J. Green, G. Freyer, A. Canion, J. Delgardio, N. Norton, T. C. Hazen and M. Huettel, *Appl. Environ. Microbiol.*, 2011, **77**, 7962–7974.
5 M. C. Redmond and D. L. Valentine, *Proc. Natl. Acad. Sci. U. S. A.*, 2012, **109**, 20292–20297.
6 H. Zhu, S. Qiu, W. Jiang, D. Wu and C. Zhang, *Environ. Sci. Technol.*, 2011, **45**, 4527–4531.
7 O. U. Mason, T. C. Hazen, S. Borglin, P. S. G. Chain, E. A. Dubinsky, J. L. Fortney, J. Han, H.-Y. N. Holman, J. Hultman and R. Lamendella, *ISME J.*, 2012, **6**, 1715–1727.
8 T. Arbatan, X. Fang and W. Shen, *Chem. Eng. J.*, 2011, **166**, 787–791.
9 W. M. Graham, R. H. Condon, R. H. Carmichael, I. D'Ambra, H. K. Patterson, L. J. Linn and F. J. Hernandez Jr, *Environ. Res. Lett.*, 2010, **5**, 045301.
10 A. R. Pendashteh, A. Fakhru'l-Razi, S. S. Madaeni, L. C. Abdullah, Z. Z. Abidin and D. R. A. Biak, *Chem. Eng. J.*, 2011, **168**, 140–150.
11 Q. Li, C. Kang and C. Zhang, *Process Biochem.*, 2005, **40**, 873–877.
12 E. Yuliwati and A. F. Ismail, *Desalination*, 2011, **273**, 226–234.
13 J. Rubio, M. L. Souza and R. W. Smith, *Miner. Eng.*, 2002, **15**, 139–155.
14 M. Hightower, L. Gritzo, A. Luketa-Hanlin, J. Covan, S. Tieszen, G. Wellman, M. Irwin, M. Kaneshige, B. Melof and C. Morrow, *Guidance on risk analysis and safety implications of a large liquefied natural gas (LNG) spill over water*, DTIC Document, 2004.
15 J. Zhong, X. Sun and C. Wang, *Sep. Purif. Technol.*, 2003, **32**, 93–98.
16 M. R. Kumar, C. V. Koushik and K. Saravanan, *Elixir Chem. Engg.*, 2013, **54A**, 12713–12717.
17 V. K. Gupta, A. Rastogi and A. Nayak, *J. Colloid Interface Sci.*, 2010, **342**, 135–141.
18 M. H. Tai, P. Gao, B. Y. L. Tan, D. D. Sun and J. O. Leckie, *ACS Appl. Mater. Interfaces*, 2014, **6**, 9393–9401.
19 M. Yeber, E. Paul and C. Soto, *Desalin. Water Treat.*, 2012, **47**, 295–299.
20 Q. Huang, F. Mao, X. Han, J. Yan and Y. Chi, *Energy Fuels*, 2014, **28**, 4918–4924.
21 X. Xu and X. Zhu, *Chemosphere*, 2004, **56**, 889–894.
22 K. Scott, *Handbook of industrial membranes*, Elsevier, 1995.
23 C. Feng, K. C. Khulbe, T. Matsuura, S. Tabe and A. F. Ismail, *Sep. Purif. Technol.*, 2013, **102**, 118–135.
24 M. T. Ravanchi and A. Kargari, *New advances in membrane technology*, INTECH Open Access Publisher, 2009.
25 A. K. Pabby, S. S. H. Rizvi and A. M. S. Requena, *Handbook of membrane separations: chemical, pharmaceutical, food, and biotechnological applications*, CRC press, 2015.
26 M. D. Afonso and R. Borquez, *Desalination*, 2002, **142**, 29–45.
27 S. Kaur, D. Rana, T. Matsuura, S. Sundarrajan and S. Ramakrishna, *J. Membr. Sci.*, 2012, **390**, 235–242.
28 K. Yoon, B. S. Hsiao and B. Chu, *J. Membr. Sci.*, 2009, **326**, 484–492.
29 N. Bhardwaj and S. C. Kundu, *Biotechnol. Adv.*, 2010, **28**, 325–347.
30 A. Greiner and J. H. Wendorff, *Angew. Chem., Int. Ed.*, 2007, **46**, 5670–5703.
31 Z. Zhao, J. Zheng, M. Wang, H. Zhang and C. C. Han, *J. Membr. Sci.*, 2012, **394**, 209–217.
32 F. E. Ahmed, B. S. Lalia and R. Hashaikeh, *Desalination*, 2015, **356**, 15–30.
33 J. J. Doyle, S. Choudhari, S. Ramakrishna and R. P. Babu, *Conference Papers in Materials Science*, 2013, 269313–269326.
34 X. Wang, D. Fang, K. Yoon, B. S. Hsiao and B. Chu, *J. Membr. Sci.*, 2006, **278**, 261–268.
35 L. T. S. Choong, Y.-M. Lin and G. C. Rutledge, *J. Membr. Sci.*, 2015, **486**, 229–238.
36 R. Halaui, A. Moldavsky, Y. Cohen, R. Semiat and E. Zussman, *J. Membr. Sci.*, 2011, **379**, 370–377.
37 J. Lin, Y. Shang, B. Ding, J. Yang, J. Yu and S. S. Al-Deyab, *Mar. Pollut. Bull.*, 2012, **64**, 347–352.
38 I. G. Beskardes and M. Gumusderelioglu, *J. Bioact. Compat. Polym.*, 2009, **24**, 507–524.
39 D. Kessler and P. Theato, *Langmuir*, 2009, **25**, 14200–14206.
40 X. Wang, H. Hu, Q. Ye, T. Gao, F. Zhou and Q. Xue, *J. Mater. Chem.*, 2012, **22**, 9624–9631.
41 M. Guo, B. Ding, X. Li, X. Wang, J. Yu and M. Wang, *J. Phys. Chem. C*, 2009, **114**, 916–921.
42 J. Lin, F. Tian, Y. Shang, F. Wang, B. Ding, J. Yu and Z. Guo, *Nanoscale*, 2013, **5**, 2745–2755.
43 Y. Shang, Y. Si, A. Raza, L. Yang, X. Mao, B. Ding and J. Yu, *Nanoscale*, 2012, **4**, 7847–7854.

44 H. Che, M. Huo, L. Peng, T. Fang, N. Liu, L. Feng, Y. Wei and J. Yuan, *Angew. Chem.*, 2015, **54**, 8934–8938.
45 M. Obaid, G. M. Tolba, M. Motlak, O. A. Fadali, K. A. Khalil, A. A. Almajid, B. Kim and N. A. Barakat, *Chem. Eng. J.*, 2015, **259**, 449–456.
46 H. Makino and M. Nakatani, *US Pat.*, 4, 690, 873, 1987.
47 L. Liu, S. Jiang, Y. Sun and S. Agarwal, *Adv. Funct. Mater.*, 2015, **26**, 1021–1027.
48 S.-I. Moon, I. Taniguchi, M. Miyamoto, Y. Kimura and C.-W. Lee, *High Perform. Polym.*, 2001, **13**, S189–S196.
49 S. V. Vinogradova, V. V. Korshak, Y. S. Vygodskii and V. I. Zaitsev, *Polym. Sci. U.S.S.R.*, 1967, **9**, 731–736.
50 S. Rana and J. W. Cho, *Fibers Polym.*, 2011, **12**, 721–726.
51 F. Kayaci, C. Ozgit-Akgun, I. Donmez, N. Biyikli and T. Uyar, *ACS Appl. Mater. Interfaces*, 2012, **4**, 6185–6194.
52 M. K. Bernett and W. A. Zisman, *J. Phys. Chem.*, 1960, **64**, 1292–1294.
53 W. K. Cho, S. Park, S. Jon and I. S. Choi, *Nanotechnology*, 2007, **18**, 395602.
54 H. Cao, H. Zheng, K. Liu and J. H. Warner, *ChemPhysChem*, 2010, **11**, 489–494.
55 X. Wang, J. Wang, Y. Si, B. Ding, J. Yu, G. Sun, W. Luo and G. Zheng, *Nanoscale*, 2012, **4**, 7585–7592.
56 M. Ma, M. Gupta, Z. Li, L. Zhai, K. K. Gleason, R. E. Cohen, M. F. Rubner and G. C. Rutledge, *Adv. Mater.*, 2007, **19**, 255–259.
57 J.-M. Lim, G.-R. Yi, J. H. Moon, C.-J. Heo and S.-M. Yang, *Langmuir*, 2007, **23**, 7981–7989.
58 J. Y. Huang, S. H. Li, M. Z. Ge, L. N. Wang, T. L. Xing, G. Q. Chen, X. F. Liu, S. S. Al-Deyab, K.-Q. Zhang and T. Chen, *J. Mater. Chem. A*, 2015, **3**, 2825–2832.
59 M. Huang, Y. Si, X. Tang, Z. Zhu, B. Ding, L. Liu, G. Zheng, W. Luo and J. Yu, *J. Mater. Chem. A*, 2013, **1**, 14071–14074.
60 A. Al-Amoudi, P. Williams, A. Al-Hobaib and R. W. Lovitt, *Appl. Surf. Sci.*, 2008, **254**, 3983–3992.
61 B. Chakrabarty, A. Ghoshal and M. Purkait, *J. Membr. Sci.*, 2008, **325**, 427–437.